ELSA/7-2005

Proposal to the PAC

Measurement of the Helicity Difference in $\pi^0\,\eta$-Photoproduction with the Crystal Barrel Detector at ELSA

The Crystal Barrel Collaboration @ ELSA

Spokesperson: H. Schmieden
Contact Persons: V. Credé, V. Hannen, U. Thoma
e-mail: crede@fsu.edu, hannen@physik.uni-giessen.de, thoma@iskp.uni-bonn.de

C. Carasco, I. Jaegle, B. Krusche, T. Mertens
Physikalisches Institut, Universität Basel

J. Heckmann, Ch. Heß, W. Meyer, E. Radke, G. Reicherz
Physikalisches Institut, Universität Bochum

J. Barth, H. Dutz, D. Elsner, R. Ewald, K. Fornet-Ponse, S. Goertz, S. Kammer, V. Kleber, Frank Klein, Fritz Klein, M. Konrad, C. Morales, M. Ostrick, A. Raccanelli, H. Schmieden, A. Süle, D. Walther
Physikalisches Institut, Universität Bonn

O. Bartholomy, R. Beck, S. Böse, K. Essig, M. Fuchs, Ch. Funke, M. Grüner, E. Gutz, Ph. Hoffmeister, I. Horn, J. Junkersfeld, H. Kalinowsky, E. Klempt, M. Lang, M. Rost, Ch. Schmidt, T. Szczepanek, A. Thiel, U. Thoma, Ch. Wendel
Helmholtz Institut für Strahlen- und Kernphysik, Universität Bonn

A. Anisovich, D. E. Bayadilov, Yu. A. Beloglazov, A. B. Gridnev, I. V. Lopatin, D. V. Novinskiy, V. Nikonov, A. Sarantsev
Petersburg Nuclear Physics Institute, Gatchina
and Helmholtz Institut für Strahlen- und Kernphysik, Universität Bonn

P. Drexler, V. Hannen, F. Hjelm, M. Kotulla, K. Makonyi, V. Metag, M. Nanova, R. Novotny, H. van Pee, V. Sokhoyan, M. Thiel, D. Trnka
Physikalisches Institut, Universität Giessen

V. Crede
Florida State University, Tallahassee

Bonn, August 29, 2005

Beam & Target specifications:

e^- beam	3.2 GeV, 2.4 GeV e^- polarized (circ. pol. γ)
target:	polarized Butanol target
e^- beam	3.2 GeV e^- unpolarized
target:	unpolarized hydrogen target
beam line:	CB beamline
beam intensity:	$\sim 1 \cdot 10^7$ tagged photons/s

Equipment:

The measurements will take place in the former ELAN/GDH area at ELSA using the Crystal Barrel detector complemented by two new forward detectors, the so called Forward Plug and the Mini-TAPS array. These two detectors cover a forward angular range of $\pm 30°$. The Forward Plug consists of 90 CsI(Tl) crystals read out by photomultipliers, and covering the angular range between 12° and 30°. The Mini-TAPS array (216 BaF_2-crystals) covers the angular range further down to 1°. In both cases, scintillators are placed in front of the crystals to identify charged particles. In addition, a scintillating fiber detector surrounding the target will be used for charged particle tracking. Both forward detector components and the scintillating fiber detector will be included in the first level trigger. The second level trigger will be provided by FACE, a fast cluster encoder based on a cellular logic chip, which allows to trigger on the number of clusters in the Crystal Barrel and the Forward Plug.
A tagged–photon beam will be provided by the newly set up tagging system consisting of 96 scintillators and an array of 480 scintillating fibers used already for tagging purposes during the CB-TAPS beam-time. This system allows to tag photons with energies from 18 % to 95 % of the incoming electron energy.
Circularly–polarized photons will be produced using a polarized–electron beam from ELSA. The Bonn frozen spin butanol target will be used to provide logitudinally–polarized protons. The latter has a length of 2 cm whereas for the measurements without target polarization the existing LH_2-target of 5 cm length will be used.

Abstract

The search for so–called missing resonances, i.e. experimentally not established baryon states which are predicted by constituent quark models, is a long–standing challenge in hadron physics. Nearly all existing data on non–strange production of baryon resonances result from Nπ scattering experiments. However, quark models predict strong couplings of the missing states to γp as well as to single–meson final states like Nη, Nη', Nρ, Nω, but also, especially at higher energies, to two–meson final states such as N$\pi\pi$ or N$\pi\,\eta$ (e.g. via the reaction chain $\gamma p \rightarrow \Delta^* \rightarrow \Delta\eta \rightarrow p\pi^0\,\eta$). As the c.m. energy increases towards 2.0 GeV and beyond, the two– and even three–meson final states become more dominant, and it is in this important energy region that the masses and partial widths of baryon resonances are poorly determined. Thus, photoproduction experiments investigating final states like $\Delta\pi$ and $\Delta\eta$ exhibit a large discovery potential for the missing states, if these states really exist.

Polarization observables are an important ingredient to identify these states. In many cases, resonances reveal themselves more clearly through interference with dominant amplitudes. These interference terms can be isolated via polarization observables. The closer one gets to a complete experiment the fewer ambiguities remain in the partial wave analyses used to extract the properties of contributing resonances from the data.

We propose to investigate the reaction $\gamma p \rightarrow p\pi^0\eta$ using the ELSA photon beam facility and the Crystal Barrel (CB) Detector together with its two newly installed forward detectors the Forward–Detector Plug and the Mini–TAPS array. This detector setup allows to measure multi-photon final states with a large acceptance. We will make use of the longitudinally–polarized target which will be installed in the new experimental area of the CB–Detector at the GDH beamline providing polarized and unpolarized electrons. We intend to measure single and double–polarization observables. These measurements will provide new information and therefore additional contraints for the partial wave analysis (PWA). The measurements will cover almost the full angular range at center of mass energies ranging from threshold up to $\sqrt{s} = 2.56$ GeV. We will provide data of unprecedented quality and kinematical coverage suitable for coupled–channel analyses which is one of the key techniques for progress in the study of baryon resonances.

1 Introduction

The spectrum and the properties of excited baryons reflect the behavior of QCD in the low–energy regime, where the QCD Lagrangian cannot be solved by a perturbative expansion. On the one hand, lattice QCD calculations have started showing promising results. On the other hand, constituent quark models have been developed in order to describe the experimental findings. Common to these models is the use of a confining potential in combination with a short–range residual interaction. The latter differs among the various models, the most prominent examples are one–gluon exchange [1], Goldstone boson exchange [2], and instanton–induced interactions [3]. Although these constituent quark models use somewhat different approaches, they are quite succesful in generally describing the masses of low–lying states. At higher energies however, many of the predicted excited baryon states do not seem to be realized in nature. The following reasons might account for this phenomenon:

- $N\pi$ scattering experiments have been the dominant source of information until very recently. If the so–called missing resonances couple only weakly to $N\pi$, they will not be observed in this process.
- Photoproduction data was up to now mainly available up to a center–of–mass energy of $1800\,\mathrm{MeV}/c^2$. The missing resonance problem appears in the region above this value.
- Polarization experiments have so far been performed mainly in the low energy region, e.g. at GRAAL, LEGS and MAMI. The use of polarization, however, is crucial at higher energies where resonances strongly overlap. Single and double polarization information will lead to additional constraints in the partial wave analysis. A first step into this direction has already been done with the CB-ELSA/TAPS experiment where linearly–polarized photons were produced with energies up to 2 GeV.
- Many channels with more than one meson in the final state are still not explored. High–lying resonances may not decay directly into the nucleon ground state via single meson emission but via a sequential decay chain. In such a chain, intermediate states may be populated that exhibit only a weak photon coupling.
- The quark model predicts a level density that becomes increasingly dense at energies above 2 GeV and it is an open question if such a high population of states is reasonable. One way to explain a reduced level density would be a deeply bound diquark [4] but also other explanations have been suggested [5]. To make progress on this issue a good knowledge of the high–mass baryon spectrum is needed.

But even in the low–mass region, constituent quark models exhibit severe problems. For example, the masses of the low–lying radial excitations of the nucleon or of the $\Delta(1232)$ do not match the predictions. These are the $\mathrm{N}(1440)\mathrm{P}_{11}$ and the $\Delta(1600)\mathrm{P}_{33}$, respectively. Another example are the negative–parity Δ states with masses around 1900 MeV. These Δ resonances, i.e. $\Delta(1900)\,\mathrm{S}_{31}$, $\Delta(1940)\,\mathrm{D}_{33}$ and $\Delta(1930)\,\mathrm{D}_{35}$, are expected at significantly higher masses by the constituent quark models.

In addition, there are other phenomenological observations which are only poorly un-

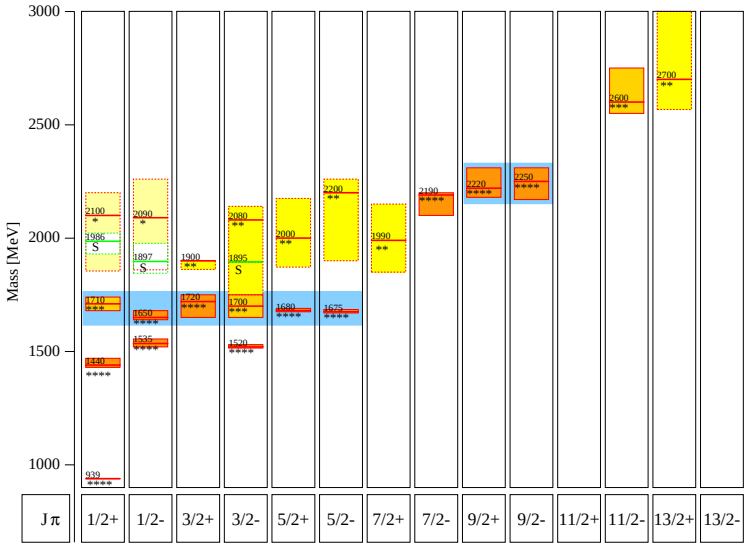

Figure 1: Spectrum of N* states, the blue boxes indicate the occurance of parity doublets.

derstood. For example, in the N and Δ excitation spectrum indications for parity doublets are found, i.e. states of equal total angular momentum but with opposite parity being almost degenerate in mass. In Ref. [6], it has been suggested that the parity–doublet structure observed in the spectrum of excited baryons may be due to effective chiral restoration in the limit of large excitation energies. Other models explain the parity doubling in terms of the quark dynamics leading to different predictions [7, 8]. In many cases, the effect is striking: states with identical J but opposite parity often have very similar masses (see Fig. 1). Among constituent quark models, only those based on instanton–induced forces [3] describing the short–range interaction between quarks account naturally for this effect.

Over the last decade, indications for only a few new resonances have been reported. The $\gamma\,\mathrm{p} \rightarrow \mathrm{p}\,\eta'$ SAPHIR data propose the existence of a third S_{11} at 1890 MeV and a P_{11} at 1980 MeV [9]. In [10], it was shown that the data could also be described without an additional P_{11}. Here, the S_{11} is interfering with the Regge–trajectory exchanges. In the $\gamma\,\mathrm{p} \rightarrow \mathrm{K}^+\,\Lambda$ SAPHIR data [11, 12], evidence for an additional D_{13} resonance with a mass of about 1900 MeV [13] was found. Recently, high–statistics data on the reactions $\gamma\mathrm{p} \rightarrow \mathrm{K}^+\Lambda$, $\gamma\mathrm{p} \rightarrow \mathrm{K}^+\Sigma^0$, and $\gamma\mathrm{p} \rightarrow \mathrm{K}^0\Sigma^+$ have been measured by the SAPHIR [12, 14], CLAS [15], and LEPS [16] collaborations for center-of-mass energies between 1.6 and 2.3 GeV. A combined partial wave analysis of these data with additional π and η photoproduction data from CB-ELSA and a variety of other sources reveals evidence for a $\mathrm{P}_{11}(1840)$ and for two D_{13} states at 1875 MeV and, optimistically, at 2170 MeV [17]. In this analysis, which also included the new CB-ELSA η [18] and π^0 photoproduction data [19], evidence for a further state, $\mathrm{D}_{15}(2070)$, coupling strongly to $\mathrm{p}\eta$ was found [20].

While the $\mathrm{D}_{15}(2070)$, the $\mathrm{D}_{13}(1875)$, and the $\mathrm{D}_{13}(2170)$ fit nicely to the quark model predictions (Fig. 2), this is not true for the $\mathrm{P}_{11}(1840)$. The possible existence of an additional P_{13} state around 1700 in CLAS electroproduction data would also be in

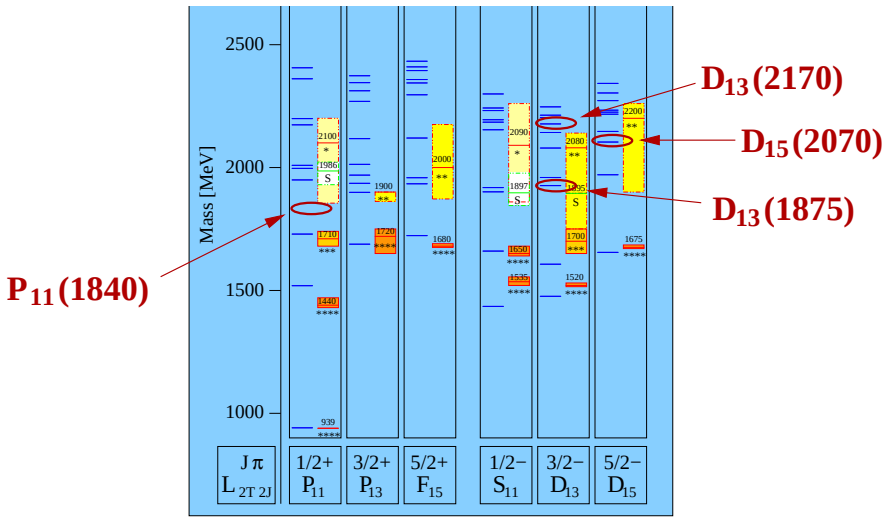

Figure 2: New resonances found in the partial wave analysis by the Bonn group [17, 20].

disagreement with the quark model expectations [21].

2 Motivation

Missing Resonances

In recent years, results in baryon spectroscopy indicate that 3–body final states are very likely to be the key for the discovery of higher–lying missing states because they account for most of the cross section above $W \approx 1.7$ GeV. Highly excited baryon states are predicted to decay into particles with higher masses, i.e. excited intermediate states rather than into a ground–state nucleon and a meson. Calculations of decays for those resonances into channels like $N\pi$, $N\eta$ and $N\omega$ yield small partial widths. However, high–mass states have total widths of at least 150 MeV, thus the remaining decay strength must be observed in reactions with higher thresholds. In the past, 2–body final states have been largely explored. Nonetheless, many questions in the field of single–meson production are still awaiting an answer and the planned polarization program on different final states is a scientific must. Among other things, it is of interest to see the new $D_{15}(2070)$, observed in η photoproduction [18, 22], confirmed in the proposed double–polarization experiments. These measurements are subject of two accompanying proposals (ELSA/1-2005 and ELSA/2-2005).

Although many resonances are missing in the baryon spectrum, they are difficult to establish experimentally since the number of resonances and their widths increase with mass, thus leading to many overlapping states. The investigation of mainly neutral decay channels has the particular advantage of suppressing non–resonant background, e.g. t–channel exchange processes. The high resolution of the Crystal–Barrel Detector for photons and the measurement of single and double–polarization observables will definitely help to disentangle the various contributions.

Also well–known resonances are expected to have significant couplings to $N\pi\eta$ and non–zero photoproduction amplitudes. These states will provide anchors for our analyses.

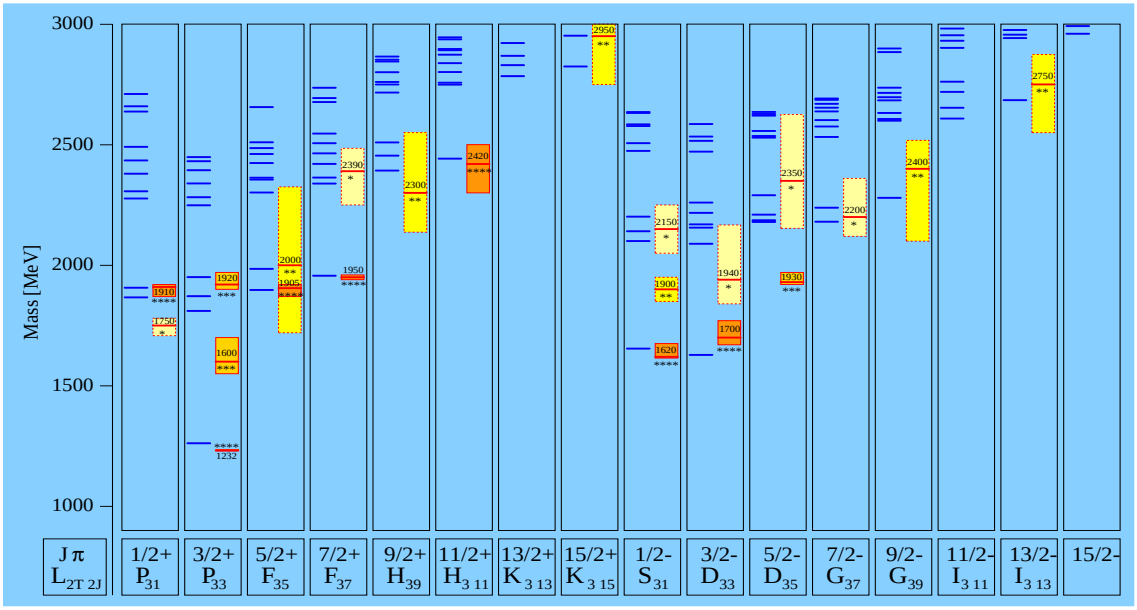

Figure 3: Predicted spectrum of Δ^* states using a relativistic quark model (left side of each column) which takes instanton induced forces into account [3]. Also given are the measured states including their PDG star ranking (right side of each column).

That is, in order to trust any identification of previously unknown states, we will pick out some of the better known states and determine their properties.

Negative–Parity Δ States

The isospin–selective reaction $\gamma p \to \Delta\,\eta \to p\pi^0\eta$ facilitates the investigation of Δ^* states with masses above the effective reaction thresholds of $1620\,\mathrm{MeV}/c^2$. The analysis of these data will shed some light on the existence of Δ^* resonances with negative parity at masses of about 1900 MeV. A confirmation of these poorly established states would be in contradiction with current constituent quark models which predict these states approximately 150–250 MeV higher in mass.

Parity Doublets

Table 1 shows some N^* and Δ^* masses above 1.9 GeV for states with positive and negative parity. In many cases, the effect of parity doubling is striking: states with identical J but opposite parity often have very similar masses. This need not imply that chiral symmetry restoration is the reason for the occurence of parity doublets. Consider e.g. the first six Δ states in Table 1 with $J = 1/2,\ 3/2$, and $5/2$, and with positive and negative parities. The masses are clearly degenerate; they form three parity doublets. The $\Delta_{7/2^+}(1950)$ and the $\Delta_{7/2^-}(2200)$ should also form a parity doublet but the $\Delta_{7/2^+}(1950)$ has a mass which is very close to the other three positive–parity resonances; it does not really fit to the $\Delta_{7/2^-}(2200)$. The four positive–parity resonances rather seem to belong to a spin quartet of states with intrinsic orbital angular momentum $L = 2$ and intrinsic spin $S = 3/2$ coupling to $J = 1/2, ..., 7/2$. On the other hand, the negative–parity states form a triplet with $L = 1$ and intrinsic spin $S = 3/2$. The question arises if the parity doublets are really due to restoration of

$J = \frac{1}{2}$	$N_{1/2^+}(2100)$	$N_{1/2^-}(2090)$	$\Delta_{1/2^+}(1910)$	$\Delta_{1/2^-}(1900)$
$J = \frac{3}{2}$	$N_{3/2^+}(1900)$	$N_{3/2^-}(2080)$	$\Delta_{3/2^+}(1920)$	$\Delta_{3/2^-}(1940)$
$J = \frac{5}{2}$	$N_{5/2^+}(2000)$	$N_{5/2^-}(2200)$	$\Delta_{5/2^+}(1905)$	$\Delta_{5/2^-}(1930)$
$J = \frac{7}{2}$	$N_{7/2^+}(1990)$	$N_{7/2^-}(2190)$	$\Delta_{7/2^+}(1950)$	$\Delta_{7/2^-}(2200)$
$J = \frac{9}{2}$	$N_{9/2^+}(2220)$	$N_{9/2^-}(2250)$	$\Delta_{9/2^+}(2300)$	$\Delta_{9/2^-}(2400)$

Table 1: Parity doublets of N^* and Δ^* resonances at higher masses, according to [6, 8].

chiral symmetry or if the parity doublets reflect a symmetry of the underlying quark dynamics. Only an experimental investigation of the high–mass baryon spectrum can decide whether each of the states has its parity partner or whether the parity doubling can be explained in terms of the quark dynamics [7, 8].

$\Delta\eta$ Decays of Resonances

There exists no information on the $\Delta\eta$ decay of any of the resonances listed by the PDG. Therefore, this decay mode provides completely new information on the observed resonances. Are there e.g. specific resonances which couple strongly to the $\Delta\eta$ channel while others do not? Such a behavior is for example observed in the $p\eta$ channel, where the $S_{11}(1535)$ couples strongly to $p\eta$ while this is not true for the $S_{11}(1650)$. This observation generated a lot of discussion on the nature of the $S_{11}(1535)$ [23, 24, 25, 26, 27, 28], reaching from a usual 3q state to a resonance generated by coupled–channel dynamics.

Evidence for the $\Delta\eta$ decay of resonances was found in the analysis of unpolarized CB-ELSA data, as discussed in the next section. Possible indications for a $\Delta\eta$ decay of the $D_{33}(1700)$ have also been reported by [29].

Search for Resonances Decaying into $S_{11}(1535)\pi$ or $pa_0(980)$

Heavy baryon resonances may also decay into $S_{11}(1535)\pi$ or $pa_0(980)$. First indications for such decays have been observed in the CB-ELSA data on $\gamma p \to p\pi^0\eta$. Surprisingly enough, it seems that $a_0(980)$ is not dominatly produced by t–channel exchange, but also by the decays of higher–mass resonances.

2.1 Theoretical Predictions

In view of this proposed program, it is important to focus some attention on models of baryon physics which are capable of providing detailed information pertinent to these experiments. In an earlier article of Capstick and Roberts [30], a study of the baryon spectrum was reported which focused on the $N\pi$ couplings of baryon states. The purpose there was twofold: to test an existing model of the baryon spectrum [1] by looking more carefully at its predictions for the strong decays, and to investigate a previously proposed solution to the problem of the missing baryons [31]. The conclusions were (i) that the model works quite well in describing the $N\pi$ decays of baryon resonances, and (ii) that, as suggested in [31], the missing baryons consistently couple only weakly to the $N\pi$ channel, and so should be sought elsewhere.

The differential cross sections for example of $\gamma\,\mathrm{p} \to \mathrm{p}\,\mathrm{X}$ ($\mathrm{X} = \pi$, η, ω) show a strong forward peaking at higher energies which is generally interpreted as production by meson exchange in the t channel. Contributions by s–channel resonance production are small. However, high–mass states still have total widths of at least 150 MeV, thus the remaining decay strength must be observed in reactions with higher thresholds. Therefore, the investigation of $\mathrm{p}\pi^0\eta$ has a big advantage in the search for missing states, especially in the search for missing Δ states. In [33], it is shown that a number of states could be verified in such an analysis, e.g. $\Delta(2000)\mathrm{F}_{35}^{**}$ and the fourth missing P_{33} resonance in the $\mathrm{p}\pi^0\eta$ channel.

As mentioned in the introduction, three negative–parity Δ states with masses around 1900 MeV are expected at significantly higher masses by constituent quark models. These are the Δ resonances $\Delta(1900)\mathrm{S}_{31}$, $\Delta(1940)\mathrm{D}_{33}$, and $\Delta(1930)\mathrm{D}_{35}$. Table 2 shows predictions of negative–parity states in the Capstick model [32]. The first row would

model state	$\mathrm{N}\,\pi$	$\sqrt{\Gamma^{\mathrm{tot}}_{\Delta\,\pi}}$	$\sqrt{\Gamma^{\mathrm{tot}}_{\Delta\,\eta}}$	$A^{p,n}_{1/2}$	$A^{p,n}_{3/2}$
$[\Delta\frac{5}{2}^-]_1(2155)$	5.2 ± 0.1	$4.0^{+0.2}_{-0.3}$	1.1 ± 0.3	11	19
$[\Delta\frac{5}{2}^-]_2(2165)$	0.6 ± 0.1	$8.1^{+3.1}_{-2.1}$	$3.9^{+1.3}_{-1.8}$		
$[\Delta\frac{5}{2}^-]_3(2265)$	$2.4^{+0.5}_{-0.7}$	6.5 ± 1.2	2.9 ± 0.4		
$[\Delta\frac{5}{2}^-]_4(2325)$	0.1 ± 0.1	$5.6^{+1.6}_{-1.5}$	$2.6^{+0.5}_{-0.6}$		

Table 2: **Results for decay widths and photocouplings for a few Δ resonances** *Results are for the lightest few negative–parity resonances with $J^P = 5/2^-$ in the N=3 band [32, 33, 34]. Notation for model states is $[J^P]_n$ (mass [MeV]), with J^P the spin/parity of the state and n its principal quantum number. The square of the listed amplitude yields the partial width in [MeV]. Photocouplings are in units of 10^{-3} $GeV^{-\frac{1}{2}}$.*

correspond to the experimentally found $\Delta(1930)\mathrm{D}_{35}$, however, further $[\Delta\,\frac{5}{2}^-]$ states are predicted. All of them exhibit reasonable decay widths to the $\Delta\eta$ channel and should be found in the proposed reaction. In addition, predictions for the photocouplings are given for the $[\Delta\,\frac{5}{2}^-]_1(2155)$ [34]. The parameters of the contributing resonances which can be determined in the proposed measurements allow to further test the model predictions.

2.2 Previous Measurements

Data on the reaction $\gamma\,\mathrm{p} \;\to\; \mathrm{p}\,\pi^0\,\eta$ were taken in 2000/2001 with the Crystal Barrel Detector in a first series of measurements at three different ELSA energies: $E_0 =$ 1400, 2600, and 3200 MeV. Figure 4, upper left, shows the total invariant mass for the $\mathrm{p}\,\pi^0\,\eta$ final state. No structures are visible at first sight. Different mass regions are indicated and the corresponding $\mathrm{p}\pi^0$ mass spectra given. Hints for baryon resonances decaying into $\Delta\eta$ now become visible. In the total mass region around 1700 MeV, no structure can be seen (Fig. 4, upper right). However, a clear peak at the Δ mass can be observed in the mass region around 1900 MeV (Fig. 4, middle left). We expect a series of resonances in this mass region with positive as well as with negative parity. In principle, it would be very difficult to disentangle them. However, in the $\Delta\eta$ threshold region we expect a small angular momentum between the η meson and the $\Delta(1232)$ resonance due to the centrifugal barrier. Hence, it should be possible to excite some

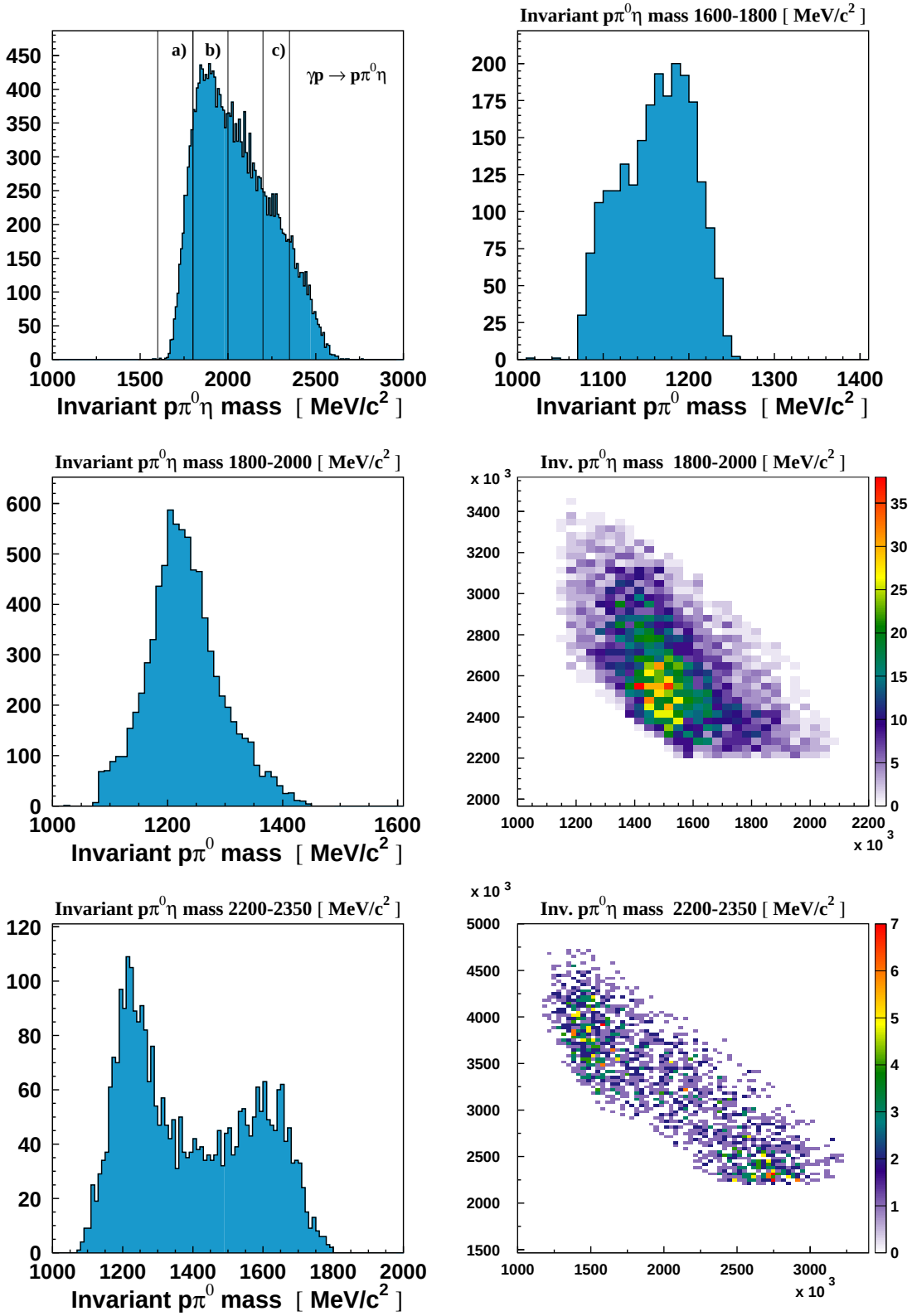

Figure 4: Different plots on the reaction $\gamma\,\mathrm{p} \rightarrow \mathrm{p}\,\pi^0\,\eta$. See text for details.

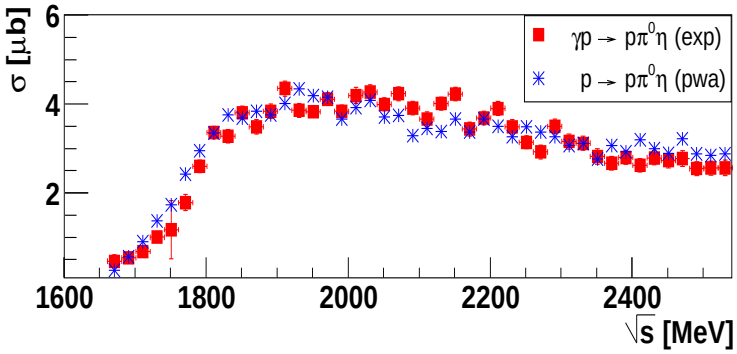

Figure 5: Total cross section for the reaction $\gamma\,\mathrm{p} \rightarrow \mathrm{p}\,\pi^0\,\eta$, the acceptance correction of the experimental data was done by a pure phase-space simulation only [35].

resonances selectively. For orbital angular momenta $l = 0$ or 1, we should expect contributions from the $\Delta(1910)\mathrm{P}_{31}$, $\Delta(1920)\mathrm{P}_{33}$, $\Delta(1905)\mathrm{F}_{35}$ ($l = 1$) and $\Delta(1940)\mathrm{D}_{33}$ ($l = 0$). For higher $\mathrm{p}\,\pi^0$ masses, further resonance intensity may be hidden in a structure around 1600 MeV (Fig. 4, lower left). Special care has to be devoted to interpreting structures in the mass projections as those are often reflections of the corresponding Dalitz plots (Fig. 4 middle right and lower right).

Fig. 5 shows the total cross section for the reaction $\gamma\,\mathrm{p} \rightarrow \mathrm{p}\,\pi^0\,\eta$. Above 2 GeV the $\gamma\,\mathrm{p} \rightarrow \mathrm{p}\,\pi^0\,\eta$ cross sections has almost the same magnitude as $\gamma\,\mathrm{p} \rightarrow \mathrm{p}\,\pi^0\,\pi^0$. Preliminary solutions of a partial wave analysis are based on an unbinned maximum likelihood fit taking all correlations among five independent variables properly into account (event–based fit). New resonances are needed to describe the data. There are hints for a new Δ state at $\approx$ 2.2 GeV and for $\Delta^* \rightarrow \mathrm{p}\,\mathrm{a}_0(980)$ as the dominant contribution for $\mathrm{a}_0(980)$ production.

In summary, a better understanding of the experimental spectrum is certainly needed. The database collected for polarization observables especially at higher energies is quite sparse. The latter will provide additional constraints for models and partial wave analyses. This also increases the sensitivity on smaller contributions and will help to distinguish between ambiguous PWA solutions.

3 Experimental Configuration

3.1 Tagging System

The new tagging system consists of 96 scintillators of varying width and a scintillating fiber array of 480 fibers (2 layers of fibers which are 2 mm in diameter). It allows to tag photons with 18 % to 95 % of the incoming electron energy with an energy resolution between 0.2 % and 2.2 %.

3.2 Polarized–Photon Beams

a) Circularly–Polarized Photon Beam

Circularly–polarized photons are produced by incoherent bremsstrahlung of longitudinally–

polarized electrons on an amorphous radiator. To determine the final polarization of the photon beam, several issues have to be considered:

- The polarization which can be reached internally in ELSA (Fig. 6)
- The loss of polarization while the polarization is rotated and the beam is extracted onto the radiator (Fig. 7, left)
- The helicity transfer from the electron to the photon (Fig. 7, right)

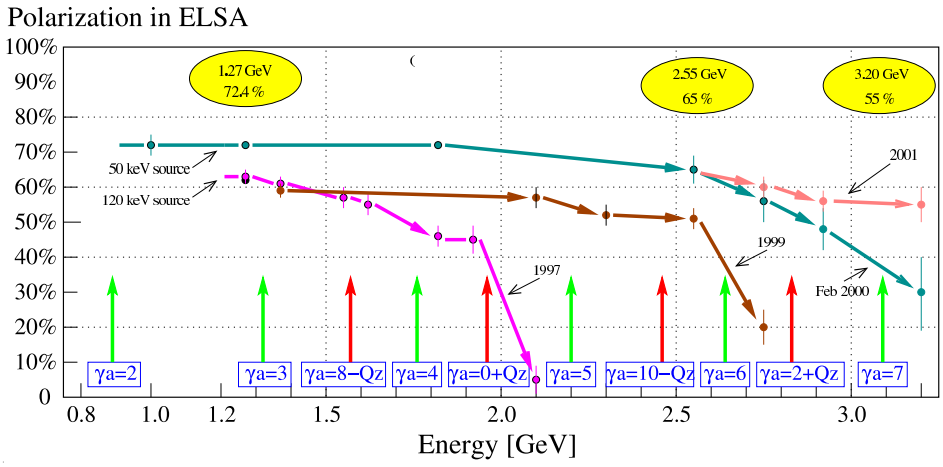

Figure 6: Polarization reached in ELSA.

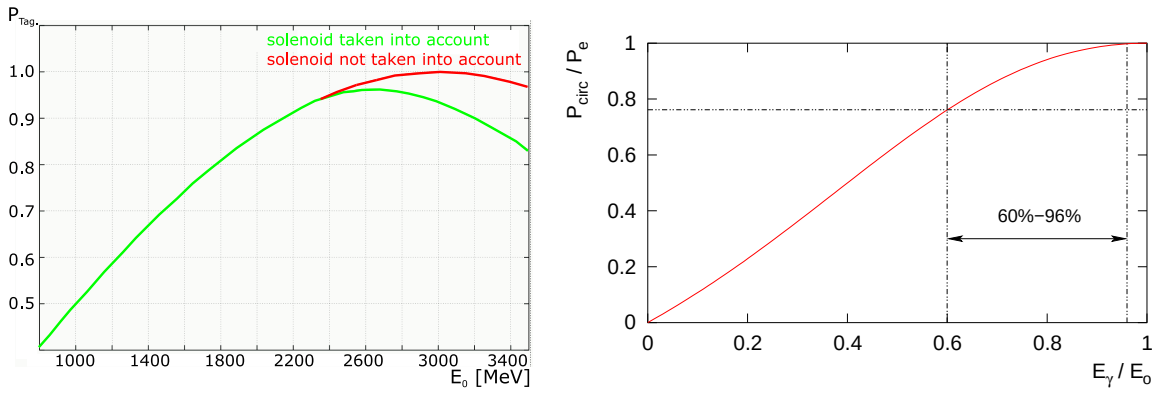

Figure 7: Left: Percentage of longitudinal polarization transferred from ELSA to the radiator target. Right: Helicity transfer $\frac{P_o}{P_e}$ from the electron to the photon.

The helicity transfer from the electron to the photon can be calculated. The polarization is approximately given by [1]:

$$P_\circ = P_{\mathrm{el}}(4z - z^2)/(4 - 4z + 3z^2)$$

z $(= E_\gamma/E_0)$ is the ratio of photon energy (E_γ) and incoming electron energy (E_0), and P_{el} is the degree of linear polarization of the incoming electrons. It is visualized

[1] A more precise calculation requires angular integration over the collimation aperture

in Fig. 7. The longitudinal polarization of the electron beam will be measured by a Møller polarimeter.

3.3 Target Polarization

In the double–polarization measurements, the Bonn frozen–spin butanol target will be used. The target uses a longitudinal holding field produced by a very thin (500 μm) superconducting solenoid located within the target cryostat which offers virtually no obstruction to the outgoing particles. The target material is butanol (C_4H_9OH) which has an effective density of 0.57 g/cm^3. In the past typical mean polarizations of 70 % were reached during the GDH beam-time. In general maximum polarizations of 90 % are possible (see also Fig. 8). The relaxation time of the target is of the order of 200 h. The target properties are summarized in more detail in Tab. 3

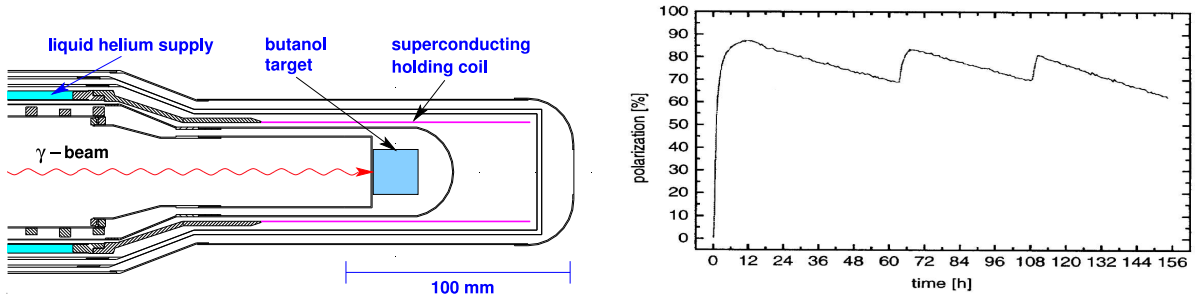

Figure 8: Polarization of the frozen–spin butanol target [36].

Material	C_4H_9OH
Dilution factor	10/74 (more exact: 0.1334 (butanol doted with porphyrexide))
Length	(18.8 ± 0.15) mm
Diameter	2 cm
Density at 1 K	0.94 g/cm^3
Filling factor	(60.7 ± 1.5) %
Density (eff.)	0.57 g/cm^3
Mean polarization	70 %
Time for repolarization	4-5 h (swap polarization +1h)
Target area density (free protons)	$8.62 \pm 0.24 \cdot 10^{22}$/ cm^2

Table 3: Parameters of the Bonn frozen–spin butanol target [37].

3.4 Detector Configuration

The Crystal Barrel detector consisting of 1230 CsI(Tl) crystals will be complemented by two new forward detector systems, the so called Forward Plug and the Mini–TAPS array, in order to perform the proposed single– and double–polarization experiments. These forward detectors close the forward angular range of $\pm 30°$, formerly covered by

the TAPS detector. The Forward Plug consists of 90 CsI(Tl) crystals covering the angular range between 30° and 12°. The Mini-TAPS array (216 BaF_2 crystals) covers the angular range further down to 1°. While the Crystal Barrel CsI(Tl) crystals are read out by photodiodes, the Forward Plug crystals will be read out by photomultipliers. The time resolution reached with the new crystal-lightguide-photomultiplier configuration is about 5 ns (FWHM) which is sufficient for its inclusion in the first level trigger.

Scintillators are placed in front of the crystals of both forward detectors to identify charged particles. For the Forward Plug, a double layer of 180 scintillators (3 mm in thickness) is placed in front of the crystals. For the Mini-TAPS detector a new configuration of scintillator plates in front of the BaF_2 crystals will be used. In contrast to the scintillators used in earlier measurements both sides of the wave length shifting fiber are read out. This increases the light output substantially.

In addition to the Crystal Barrel and the two new forward detectors described above, a scintillating fiber detector surrounding the target is used for charged particle tracking. Three layers of scintillating fibers ($\pm 25°$, $0°$) provide an intersection point of the charged particle trajectory with this detector. To give space for the polarized target in backward direction 60 crystals were removed from the Crystal Barrel. The setup of the whole detector system at ELSA as well as an enlarged view of the Crystal Barrel and the scintillating fiber detector surrounding the target together with the Mini-TAPS array are shown in Fig. 9.

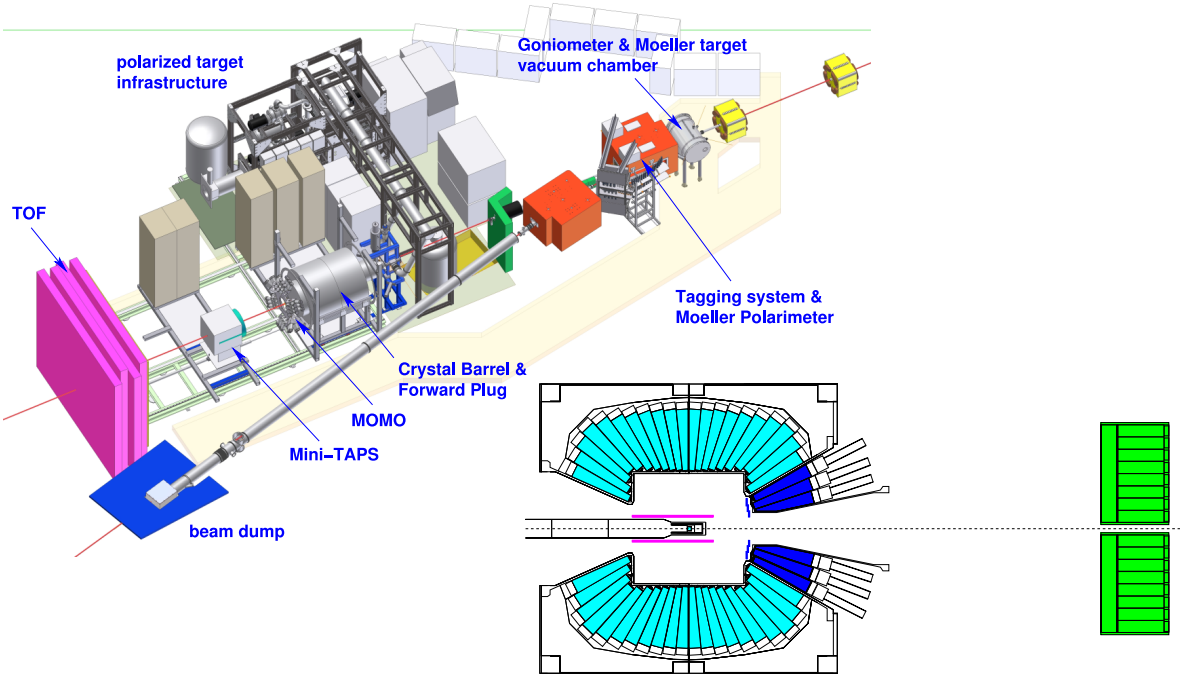

Figure 9: Experimental setup at ELSA, enlarged view on the Crystal-Barrel/inner detector and the Mini–TAPS array.

4 Analysis Techniques

Polarization observables are very important to disentangle different resonances especially at higher masses where the states strongly overlap. Here, differential cross section data, though helpful, still provide a very limited exploitation method.

4.1 Polarization Observables

The formalism and terminology for the various polarization observables of interest in double–meson photoproduction can be found in [38]. For single–meson production, the differential cross section for experiments with a polarized photon beam and a longitudinally polarized target is given by

$$\frac{\mathrm{d}\,\sigma}{\mathrm{d}\,\Omega} = \sigma_0 \left\{ 1 - \delta_l \,\mathbf{\Sigma} \cos 2\varphi - \Lambda_z \left(- \delta_l \,\mathbf{G} \sin 2\varphi + \delta_\odot \,\mathbf{E} \right) \right\}, \tag{1}$$

where σ_0 denotes the unpolarized differential cross section, δ_l is the degree of polarization for linearly polarized photons, $\delta_\odot$ is the degree of polarization for circularly polarized photons and the target polarization is given by Λ_z.

In the interesting case of two–meson or even multi–meson final states, there are more than only three different functions $\mathbf{\Sigma}$, $\mathbf{G}$, and $\mathbf{E}$ to be observed in photoproduction using polarized photons off a polarized target because many more kinematic variables are required in order to describe the system compared to single–meson production. For $\gamma\,\mathrm{p} \rightarrow \mathrm{p}\pi\eta$ without measuring the polarization of the recoiling nucleon, the reaction rate can be written as [38]:

$$\begin{aligned} \frac{\mathrm{d}\,\sigma}{\mathrm{d}\,\mathrm{x_i}} = \sigma_0 \, \{ \, (\, 1 \, - \, \Lambda_z \cdot \mathbf{P_z} \,) + \delta_\odot \, (\mathbf{I}^\odot \, - \, \Lambda_z \cdot \mathbf{E} \,) \\ - \, \delta_l \, [\sin 2\varphi \, (\, \mathbf{I^s} \, - \, \Lambda_z \cdot \mathbf{G} \,) + \cos 2\varphi \, (\, \mathbf{\Sigma} \, - \, \Lambda_z \cdot \mathbf{P_z}^{\mathbf{c}} \,) \,] \, \} \, , \end{aligned} \tag{2}$$

with the direction of polarization δ_l being at an angle φ to the reaction plane. In

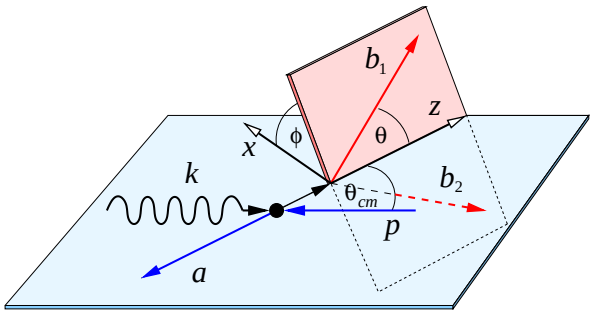

Figure 10: Decay angles in a 3-particle final state, ϕ indicates the angle between the production plane and the plane of two of the final state particles.

contrast to single–meson photoproduction, asymmetries will also occur when only the target is polarized. In case of single–meson photoproduction, the whole reaction can always be put into a single plane defined by the recoil nucleon, along with the initial photon and the target nucleon (in the center–of–mass frame). This is no longer true in the case of two or multi-meson final states, as it is indicated in Fig 10. A complete

set of experiments would require measurement of single, double and triple polarization observables, in addition to the differential cross section.

Measurements with Circularly-Polarized Beams

$$\frac{\mathrm{d}\,\sigma}{\mathrm{d}\,\mathrm{x_i}} = \sigma_0 \{ (1 - \Lambda_z \cdot \mathbf{P_z}) + \delta_\odot (\mathbf{I}^\odot - \Lambda_z \cdot \mathbf{E}) \} \tag{3}$$

In the following $\rightarrow$ and $\leftarrow$ indicate the circular polarization of the beam in its two possible settings, while $\Rightarrow$ and $\Leftarrow$ indicate the longitudinal target polarization parallel or anti-parallel to the beam.

$$(\rightarrow\Rightarrow - \leftarrow\Rightarrow): \quad \frac{\mathrm{d}\,\sigma(\rightarrow\Rightarrow)}{\mathrm{d}\,\mathrm{x_i}} - \frac{\mathrm{d}\,\sigma(\leftarrow\Rightarrow)}{\mathrm{d}\,\mathrm{x_i}} = 2 \cdot \sigma_0 \{\delta_\odot (\mathbf{I}^\odot - \Lambda_z \cdot \mathbf{E})\}$$

$$(\leftarrow\Leftarrow - \rightarrow\Leftarrow): \quad \frac{\mathrm{d}\,\sigma(\leftarrow\Leftarrow)}{\mathrm{d}\,\mathrm{x_i}} - \frac{\mathrm{d}\,\sigma(\rightarrow\Leftarrow)}{\mathrm{d}\,\mathrm{x_i}} = 2 \cdot \sigma_0 \{-\delta_\odot (\mathbf{I}^\odot + \Lambda_z \cdot \mathbf{E})\}$$

These two equations show that flipping only the beam is not sufficient to extract the double polarization observable **E**. The single polarization observable $\mathbf{I}^\odot$, only present in a three-particle final state, leads to an additional contribution. $\mathbf{I}^\odot$ does not depend on the target polarization, but it always occurs if the beam is circularly polarized.

Eqn. 4 shows that flipping the beam and the target polarization allows to measure **E** excluding the single polarization observables.

$$(\rightarrow\Rightarrow - \leftarrow\Rightarrow) + (\leftarrow\Leftarrow - \rightarrow\Leftarrow) := 4 \cdot \sigma_0 \cdot \delta_\odot \cdot \Lambda_z \cdot \mathbf{E} \tag{4}$$

Excluding the contribution $\mathbf{I}^\odot$ is of special importance since the interaction of the polarized beam with the unpolarized C_4O background leads to an unknown asymmetry. This asymmetry could otherwise only be controlled by performing a background measurement using a circularly polarized beam on an unpolarized butanol target.

Information on $\mathbf{P_z}$ can be obtained from the same measurement:

$$(\leftarrow\Leftarrow - \leftarrow\Rightarrow) - (\rightarrow\Rightarrow - \rightarrow\Leftarrow) := 4 \cdot \sigma_0 \cdot \Lambda_z \cdot \mathbf{P_z} \tag{5}$$

For the measurement of **E** and $\mathbf{P_z}$ it is of course necessary to determine the unpolarized differential cross section independently from a liquid hydrogen target, if one does not want to do background measurements to be able to determine σ_0 from the double polarization measurements.

4.2 Partial wave analysis

The main goal of a partial wave analysis is to identify the dynamical processes governing a reaction, to identify the baryon states, and to determine their quantum numbers and decay properties. This task is known to be difficult because ususally many strongly overlapping resonances contribute which may also strongly interfere with each other. In addition, background amplitudes such as Born–terms, t– and u–channel exchanges

may also play an important role and must be taken into account.

Resonances have unique characteristics such as pole positions and decay couplings into different channels, which must be identical in all reactions. Fitting a set of reactions, like e.g. the π– and photo–induced production of one and two pions, one can define a set of decay couplings which are directly connected to the width of the state.

Therefore, it is very important to do a combined analysis of different reactions and final states. The well known method of multipole decomposition is not suitable here since it cannot be directly applied to reactions with three or more particles in the final state. A fully relativistically invariant approach based on the operator expansion method was developed in Bonn [39]. It has already been applied in a combined fit of different single meson photoproduction channels together with the CB-ELSA double pion photoproduction data. In the low energy regime, the single–meson photoproduction data fixes very firmly masses, widths and helicity ratios of the dominant contributions. Some first fits of the single meson channels together with the CB-ELSA $\gamma p \to p\pi^0\eta$ channel have been performed. Also in this case, the combined fit contraints the fit better than in the single–channel analysis, which did result in a number of ambiguous solutions for the $\gamma p \to p\pi^0\eta$ channel.

The developed method is based on an event–by–event analysis. The partial wave amplitudes are constructed from the polarization and momentum 4-vectors of the initial and final state particles. For the single–meson production (for pion– and photo–induced reactions) the method can be algebraically rewritten into the standard expressions used in the partial wave analysis, like e.g. the multipole decomposition for the photoproduction. And, assuming the cascade mechanism (three body vertices only) the partial wave amplitude can be formulated for any reaction with any number of final particles.

Being event based, the method can be directly used in an event–based likelihood minimization procedure. For multibody final states, such an approach is the only way to take all correlations between the different variables the event depends on properly into account.

On the other hand, the method is also very convenient for the χ^2 fit of differential cross sections and polarization observables. For single meson production one can simulate 4-vectors which correspond to a given energy and angle and then calculate the differential cross section and polarization observables. For multibody final states the mass and angular projections of the differential cross sections and polarization observables can be calculated simultaneously with calculation of the Monte Carlo integral for unpolarized data and can then be used to fit corresponding experimental projections.

For the analysis of the double polarization data, we will perform an event based likelihood analysis of the unpolarized data obtained on an LH_2 target and a χ^2 based fit of the large set of projections of the polarization observables. Of course this fit will again be performed together with various other single meson final states, as presently included in the fit. The polarization data will be divided into sets of energy slices, extracted with different azimuthal angle dependencies and projected to the different mass and angular distributions. Although in this method some information about correlations of the polarization observables will be lost, it has many advantages. The information on the polarization observables can be extracted from data taken with a

different direction of the beam and/or target polarization as described in section 4.1, which has the advantage that the unpolarized background from the butanol drops out. Second, such method practically does not effect the speed of the program and thus, solutions can be obtained very quickly.

To perform an unbinned maximum likelihood fit it would be necessary to measure, introduce and fit the background from the unpolarized butanol nucleons. Therefore we restrict ourselves in this proposal to the above mentioned procedure.

5 Sensitivity studies

Sensitivity studies have been performed by using our partial wave analysis. To test the sensitivity of a double polarization observable on a certain resonance or partial wave, the corresponding contribution was omitted in the total amplitude and then the data re–fitted without this resonance. In a next step, the double–polarization observable in question was calculated. In the following pictures, the best fit obtained in the PWA of the unpolarized CB-ELSA data is always shown as a black solid curve.

Since the data are re–fitted after the exclusion of a certain contribution, the effects observed are of course smaller than without doing so. This method is certainly more realistic. Re–fitting the data without a certain contribution can of course have an influence on all other amplitudes. For this reason, effects can occur far above or below the mass region where the original contribution has been excluded.

In the following, some examples for the sensitivity of the double polarization observable **E** to changes in the PWA solutions are displayed. We have simulated the effects on the polarization observables for four different mass regions: 1750 MeV, 1900 MeV, 2100 MeV, and 2300 MeV. In the following, the black curve always represents the best PWA solution of unpolarized data whereas the blue and red curve show deviations from this best solution when a certain resonance contribution is omitted in the amplitude.

Energy slice 1650 - 1850 MeV

In the lowest mass region, the effects of omitting the $D_{33}(1700)$ from the fit as well as omitting the t–channel contributions have been tested. The dominant t-channel amplitude is the production of $\Delta\eta$ via ρ-meson exchange. Although the $D_{33}(1700)$ is a well known resonance, nothing is known about a possible $\Delta\eta$ decay of this state. It is therefore interesting to see what kind of effect can be observed in the double polarization observable **E** if this state is omitted from the fit. Figure 11 exhibits rather large deviations from the best PWA solution with **E** even changing sign over some regions of the invariant mass plots.

Energy slice 1800 - 2000 MeV

In the mass region around 1900 MeV/c^2, we have investigated the effects of dropping either the $\Delta(1940)D_{33}$ resonance (Figure 12 blue curves) or the $N(2100)P_{11}$ resonance (Figure 12 red curves) from the best solution. Both resonances are poorly established yet with only a one star PDG rating. Omitting the N(2100) state results in a large deviation from the best solution when looking at **E** plotted against the invariant $M_{\eta p}$ mass. Also when the $\Delta(1940)D_{33}$ resonance is dropped from the solution, measurable

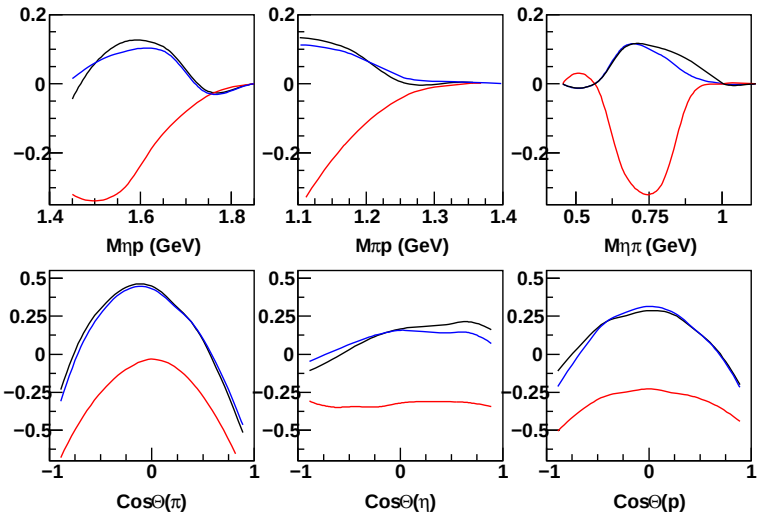

Figure 11: Comparision of PWA predictions for double–polarization observable **E**. Energy slice 1650 - 1850 MeV. Black line: best solution, red line: no $\Delta(1700)D_{33}$, blue line: no t channels.

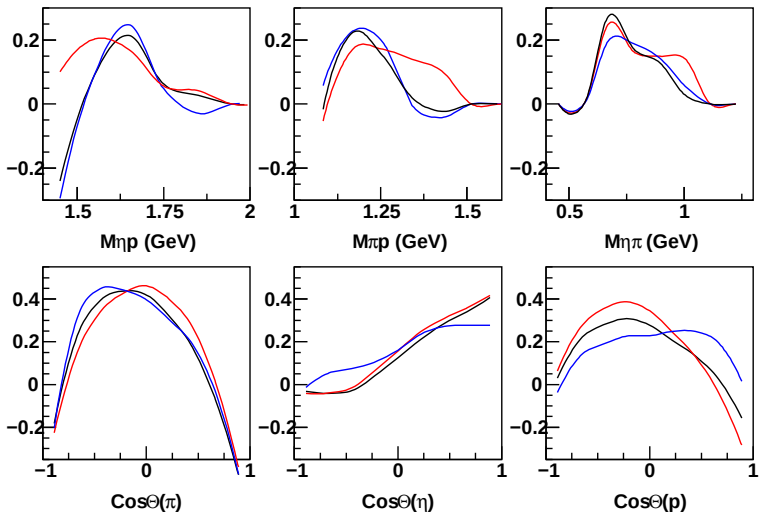

Figure 12: Comparision of PWA predictions for double–polarization observable **E**. Energy slice 1800 - 2000 MeV. Black line - best solution, red line - no $N(2100)P_{11}$, blue line - no $\Delta(1940)D_{33}$.

effects can be observed (Fig. 12, lower right plot).

Energy slice 2000 - 2200 MeV

Figure 13 depicts the same PWA solutions at higher energies. Compared to the energy range around 1900 MeV, the effects have dramatically increased and the two alternative solutions can easily be discerned from the best solution.

Energy slice 2200 - 2400 MeV

Finally in the mass region around 2300 MeV, the observable **E** has been simulated for the case when the $\Delta(1920)P_{33}$ is removed from the best solution (Figures 14 red curves) and in addition when t–channel exchanges are ignored in the solution (Figures 14 blue

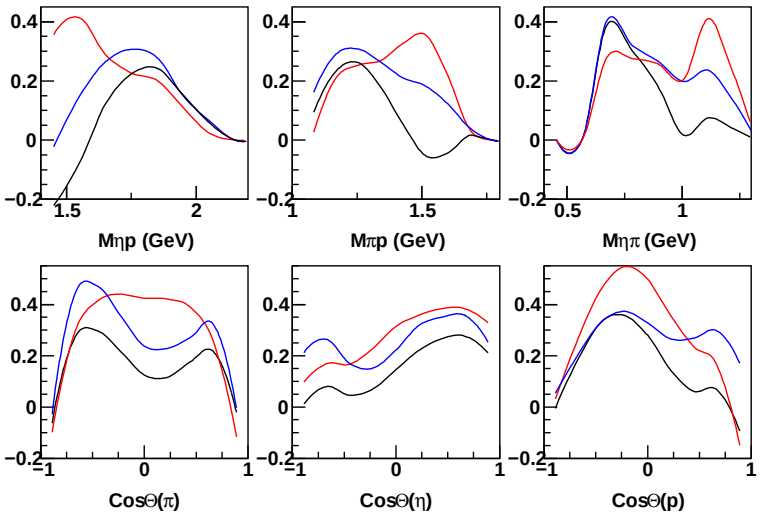

Figure 13: Comparision of PWA predictions for double polarization observable **E**. Energy slice 2000 - 2200 MeV. Black line - best solution, red line - no N(2100)P_{11}, blue line - no $\Delta(1940)D_{33}$.

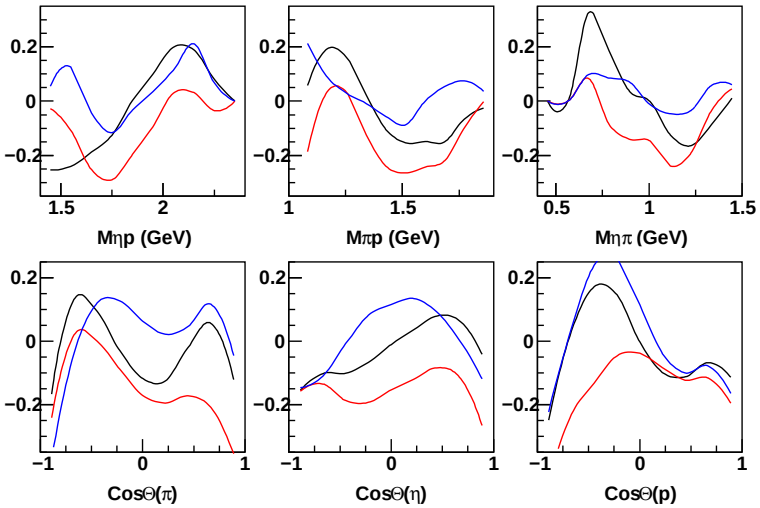

Figure 14: Comparision of PWA predictions for double polarization observable **E**. Energy slice 2200 - 2400 MeV. Black line - best solution, red line - no $\Delta(1920)P_{33}$, blue line - no t-channels.

curves). Both variations of the original solution give considerable effects.

6 Acceptance and Background Studies

6.1 Acceptance

Trigger Acceptance

The trigger acceptance has been studied in detail for the $p\pi^0$ and the $p\pi^0\pi^0$ channel and is given in the corresponding proposal on the $p\pi^0\pi^0$ final state (proposal no. ELSA/6-2005). The $p\pi^0\eta$ channel results in the same or a larger number of final state particles as the $p\pi^0\pi^0$-channel. Therefore, a very similar trigger acceptance is to be

expected. Including the inner detector, the Forward Plug, and the Mini–TAPS array into the first level trigger, it was shown that, apart from a small region of reduced acceptance for very forward going protons, the full acceptance is covered. This is still true if one asks in the second level trigger for two or more particles in the detector where at least one of them needs to be in the Crystal Barrel or Forward Plug. The obtained trigger acceptance does in addition not show any strong dependence on any of the variables the reaction depends on.

Reconstruction Efficiency

For the decay of the η meson into two photons, the reconstruction efficiency for the $\gamma p \to p\pi^0\eta$ reaction determined from measurements with the original CB-ELSA setup was found to be 15% on average. Compared to the symmetrical barrel setup used then, we gain at forward angles, where the new setup provides a coverage down to 1° polar angle. Monte Carlo simulations of the reconstruction efficiency that can be expected for the new setup are underway.

For the decay of the η meson into three pions, the reconstruction efficiency is about a factor three reduced compared to the situation described above [35].

6.2 Background

There are different sources of background to the data which need to be considered; the background from other hadronic channels, the electromagnetic background and the background stemming from the unpolarized nucleons of the target.

Hadronic Background

The four–momenta of the neutral mesons (π^0, η) are not measured directly but reconstructed from their decay products. In the absence of an inner tracking device, the η meson can be measured and its four–vector determined either from its decay into 2 photons or via the decay into $3\,\pi^0$ going to 6 photons. In case of the η decaying into 2 photons, the dominant competitor is certainly the production of two π^0's, which leads to exactly the same final state. A kinematic fit to $\pi^0\gamma\gamma$ normally shows background under the η peak of the order of 10 %. This can be further reduced by applying confidence–level anti–cuts and π^0 mass cuts in order to reject background events from $\gamma\,\mathrm{p} \to \mathrm{p}\,\pi^0\pi^0$. The remaining background is in the order of a few %.

Electromagnetic Background Rates

The interactions of photons with the butanol target are predominantly of electromagnetic nature with the main contributions stemming from pair production of electrons and positrons in the Coulomb field of the atomic nuclei and Compton scattering off orbital electrons of the atoms (see Fig. 15).

To get an estimate of the expected e.m. rates in the various detector systems and of the efficiency with which e.m. events can be suppressed by the 2nd level trigger, Geant simulations of the new setup have been performed. In the simulations, a beam of Bremsstrahlung distributed photons with energies between 1 MeV and 3.2 GeV is

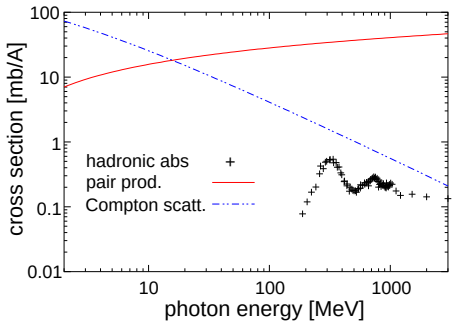

Figure 15: Electromagnetic background rates [52].

incident on the polarized target. The occurence of electromagnetic processes in the target or in any of the surrounding material is simulated by Geant according to the specific probabilities for these processes.

To determine the expected first level trigger rate stemming from e.m. events, we assume the following trigger condition: a 1st level trigger is generated when a signal from the inner detector (2 out of 3 layers required), the Forward Plug crystals or the Mini-TAPS crystals is detected in coincidence with a hit from the tagger. The tagger rate is assumed to be 10 MHz and the width of the coincidence window with the other detectors is assumed to be 40 ns. To limit the e.m. trigger rates the trigger threshold of the Mini-TAPS BaF_2 crystals has been set to 50 MeV. In addition, the innermost ring of TAPS modules has been excluded from the 1st level trigger.

The results of the simulation are summarized in table 4. Given are the total e.m. rate

	trigger threshold	total e.m. rate	random coinc.	real coinc.
Inner detector	150 keV	25 kHz	9.7 kHz	1.0 kHz
Forward Plug	15 MeV	1.8 kHz	0.6 kHz	0.4 kHz
Mini-TAPS rings 2-8	50 MeV	40 kHz	13.6 kHz	6.3 kHz
			$\Sigma = 31.5kHz$	

Table 4: E.m. rates in detectors included in the 1st level trigger decision.

above the trigger threshold of the detectors and the rate of random and real coincidences with the tagger system. The sum of real and random coincidences results in a total e.m. 1st level trigger rate of about 32 kHz. If in the 2nd level trigger we require either ≥ 2 clusters in FACE or one cluster in FACE and ≥ 1 hit in Mini-TAPS, events from the e.m. background are reduced to less than 1/600. We then end up with a rate of about 50 Hz of e.m. events that pass both the 1st and 2nd level trigger. At a 1st level trigger rate around 30 kHz the deadtime of the data acquisition system arising from the FACE processing time and from the time required for readout of hadronic events is expected to be on the order of 50%.

The possibility to place a Cherenkov counter in between the Forward Plug and the Mini-TAPS setup is currently under investigation. Such a detetector would allow to veto events with electrons or positrons going into forward direction and would therefore remove a large part of the e.m. triggers.

Background from unpolarized nucleons

Reactions on bound (unpolarized) nucleons of the target material have to be taken into account as a second potential source of background. The mean polarization for protons in a butanol target will be about $P_z = 70$ %, but the fraction of protons that can be polarized (^{1}H atoms) is just 13 % (see section 3.3). Hence, background from unpolarized nucleons in the carbon or oxygen nuclei of butanol is to be expected. The Fermi motion of these nucleons in the quasi–free kinematics contributes to a broad background underneath the missing–mass distributions for events on hydrogen. However, on applying the same reconstruction procedure as for a pure hydrogen target, the tails of this Fermi energy smearing are cut off such that the background is strongly reduced.

This has been studied in more detail for the $p\pi^0\pi^0$ final state. Data on carbon, taken with the CB/TAPS setup have been investigated and an effective dilution factor of $(D_{eff})^{-1} \approx 1.6$ has been found (for details see proposal no. ELSA/6-2005 on $\gamma p \rightarrow p\pi^0\pi^0$). Here it is assumed that the dilution factor to be expected for the $p\pi^0\eta$ final state is the same as for $p\pi^0\pi^0$. This is a reasonable assumtion since again the kinematical constraints available for determining the reaction are identical.

7 Beam Time Request

7.1 Count Rate Estimate

The rate of reconstructed $\gamma p \rightarrow p\pi^0\eta$ events originating from free protons contained in the frozen spin butanol target can be calculated using

$$N^{free}_{p\pi^0\eta} = \dot{N}_\gamma \cdot \rho^p_t \cdot \sigma^p_{tot} \cdot \epsilon \cdot \Gamma \cdot 1/N_{bins}$$

where $\dot{N}_\gamma$ is the tagged photon rate, ρ^p_t the target area density of free protons, σ^p_{tot} the total cross section for the reaction on free protons, ϵ the reconstruction efficiency and N_{bins} the desired number of bins.
Besides reactions on free protons we will also reconstruct unwanted events stemming from bound nucleons contained in the butanol molecules although with a lower reconstruction efficiency. This fact is expressed by the effective dilution factor D_{eff}. The ratio of reconstructed events from free nucleons to reconstructed events from bound nucleons is given by

$$N^{free}_{p\pi^0\eta} \,/\, N^{bound}_{p\pi^0\eta} = D_{eff}/(1 - D_{eff})$$

We can therefore calculate the total reconstructed event rate using

$$N^{tot}_{p\pi^0\eta} = N^{free}_{p\pi^0\eta} + N^{bound}_{p\pi^0\eta} = \dot{N}_\gamma \cdot \rho^p_t \cdot \sigma^p_{tot} \cdot \epsilon \cdot \Gamma \cdot 1/N_{bins}/D_{eff}$$

Inserting the following numbers

$$
\begin{array}{lcl}
\dot{N}_\gamma & = & 10 \text{ MHz} \\
\rho_t^p & = & 8.62 \cdot 10^{22}/cm^2 = 8.62 \cdot 10^{-8}/\mu\text{b} \\
\sigma_{tot}^p & = & 3.5\ \mu\text{b} \\
\epsilon & = & 15\% \text{ for } \gamma p \to p\pi^0\eta \to p\,4\gamma, \text{ branching ratio } \Gamma = 39.4\%, \\
 & & 5\% \text{ for } \gamma p \to p\pi^0\eta \to p\,8\gamma, \text{ branching ratio } \Gamma = 32.5\% \\
N_{bins} & = & 20 \text{ energy bins} \times 5 \text{ bins in } \frac{\mathrm{d}\,\sigma}{\mathrm{d}\,\mathrm{x_i}} = 100 \text{ bins} \\
(D_{eff})^{-1} & = & 1.6
\end{array}
$$

we obtain a reconstructed event rate of $N_{p\pi^0\eta}^{tot} \approx 13$ events/h/bin.

7.2 Uncertainties of the measurements

The double polarization observable E is proportional to an asymmetry $A_z^\odot$ that arises as the difference of measurements with the spins of the incoming photons either aligned with the spins of the free protons in the target material ($\rightarrow\Rightarrow$ or $\leftarrow\Leftarrow$ configuration) or opposite to the free proton spins ($\leftarrow\Rightarrow$ or $\rightarrow\Leftarrow$ configuration). If we label the number of counts obtained in these measurements with $N_\parallel$ and $N_\perp$, respectively, the asymmetry is given by

$$A_z^\odot = \frac{1}{D_{\text{eff}} \cdot \delta_\odot \cdot \Lambda_z} \frac{N_\parallel - N_\perp}{N_\parallel + N_\perp} \tag{6}$$

and the statistical error can be determined using

$$\Delta A_z^\odot(\,\text{stat.}) \approx \frac{1}{D_{\text{eff}} \cdot \delta_\odot \cdot \Lambda_z} \frac{1}{\sqrt{N_\parallel + N_\perp}}\,. \tag{7}$$

Solving for the total number of counts required to reach a certain precision $\Delta A_z^\odot(\,\text{stat.})$ we obtain

$$\Rightarrow N_\parallel + N_\perp \approx \left(\frac{1}{D_{\text{eff}} \cdot \delta_\odot \cdot \Lambda_z \Delta A_z^\odot(\,\text{stat.})} \right)^2\,. \tag{8}$$

The number of reconstructed events per bin required for measurements of single polarization observables can be obtained likewise.

At an ELSA energy of 2.4 GeV we can expect the circular photon polarization $\delta_\odot$ to be at least 46% for energies ranging from 60% to 95% of the incoming electron energy (see Figures 6 and 7). The average target polarization is assumed to be $\Lambda_z = 70\%$ and the dilution factor $(D_{eff})^{-1} = 1.6$. If we want to reach an accuracy of $\Delta A_z^\odot(\,\text{stat.}) = 0.06$ we therefore are required to collect ≈ 6900 reconstructed $\pi^0\eta$ events per bin. At a rate of 13 reconstructed events/h/bin this requires a pure measurement time of ≈ 530 h (not taking into account the deadtime of the detector or time needed to repolarize the target).

For an ELSA energy of 3.2 GeV the minimum circular photon polarization within the range of 60% to 95% of the incoming electron energy drops to $\delta_\odot = 37\%$. Relaxing the requirement on the asymmetry to $\Delta A_z^\odot(\,\text{stat.}) = 0.07$ we then need a total number of ≈ 7800 reconstructed events corresponding to a pure measurement time of ≈ 600 h.

7.3 Beam–Time Request

The following tables provide an overview of the requested beam-times for the various combinations of beam energy, beam polarization and target polarization foreseen for the measurement of double polarization observables in the $\gamma p \to p\pi^0\eta$ reaction. Given are the times T calculated purely according to the above formulas and effective times T_{eff} that take into account the dead time of the data acquisition system and the overhead required for repolarization of the polarized frozen spin target. The measurements will, as far as possible, proceed in parallel with the proposed Experiments investigating π^0, η and $\pi^0\pi^0$ photoproduction with circularly polarized photon beams (proposals no. ELSA/2-2005 and ELSA/6-2005).

Measurements with circular polarized beam

Measurements applying a circularly polarized photon beam on a longitudinally polarized target will allow to determine the single and double polarization observables **E**, and $\mathbf{P_z}$.

E_0 [GeV]	target	$\Delta\mathbf{E}$(stat.)	T [h]	T_{eff} [h]	objective
2.4	long.pol.	0.06	530	1060	measurement **E**, $\mathbf{P_z}$
3.2	long.pol.	0.07	600	1200	measurement **E**, $\mathbf{P_z}$

Table 5: Summary of the requested beam time with circularly polarized photons.

Measurements with unpolarized beam

Measurements of the unpolarized cross section on a LH_2 target are needed for the determination of the double polarization observable **E** from the measured helicity differences. The statistical error of the unpolarized measurements will contribute with less than 2% to the error of the polarization observables. In principle, the unpolarized cross section could also be obtained from the previous CB-ELSA measurements. This would however be problematic due to the differences in angular coverage and due to different systematic uncertainties of the data taken with the new and the old setups. Besides measurements with a LH_2 target we also plan to take data using an unpolarized beam on an unpolarized butanol target as part of the commissioning phase of the new setup. These data may serve to check for instrumental asymmetries of the detector and, together with the data gathered using the LH_2 target, can be used to estimate the background distribution stemming from the bound nucleons in the butanol target.

E_0 [GeV]	target	T [h]	T_{eff} [h]	objective
3.2	unpol. LH_2	120	240	normalization, D_{eff}

Table 6: Summary of the requested beam time with unpolarized photons.

References

[1] S. Capstick and N. Isgur, Phys. Rev. D34 (1986) 2809

[2] L.Ya. Glozman and D.O. Riska, Phys. Rep. 268 (1996) 263

[3] U. Loring et al., Eur. Phys. J. A10 (2001) 309

[4] D.B. Lichtenberg, Phys. Rev. **178**, 2197 (1969).

[5] E. Klempt, arXiv:hep-ph/0404270

[6] T.D. Cohen and L.Ya. Glozman, Phys. Rev. D65 (2002) 016006

[7] U. Loring and B. Metsch, hep-ph/0110412 (2001)

[8] E. Klempt, Phys. Lett. B559 (2003) 144

[9] R. Plotzke et al., Phys. Lett. B444 (1998) 555

[10] W. T. Chiang, S. N. Yang, L. Tiator, M. Vanderhaeghen and D. Drechsel, Phys. Rev. C **68**, 045202 (2003) [arXiv:nucl-th/0212106].

[11] M.Q. Tran et al., Phys. Lett. B445 (1998) 20

[12] K.H. Glander et al., Eur. Phys. J. A19 (2004) 251

[13] C. Bennhold et al., Nucl. Phys. A639 (1998) 209

[14] R. Lawall *et al.*, Eur. Phys. J. A **24** (2005) 275.

[15] J.W.C. McNabb *et al.*, Phys. Rev. C **69** (2004) 042201.

[16] R.G.T. Zegers *et al.*, Phys. Rev. Lett. **91** (2003) 092001.

[17] A. V. Sarantsev, V. A. Nikonov, A. V. Anisovich, E. Klempt and U. Thoma, arXiv:hep-ex/0506011.

[18] V. Crede et al., Phys. Rev. Lett. 94 (2005) 012004

[19] O. Bartholomy *et al.* [CB-ELSA Collaboration], Phys. Rev. Lett. **94**, 012003 (2005).

[20] A. V. Anisovich, A. Sarantsev, O. Bartholomy, E. Klempt, V. A. Nikonov and U. Thoma, arXiv:hep-ex/0506010.

[21] V.I. Mokeev et al., Yad. Fiz. 64, 1368 (2001), [Phys. At. Nucl. 64, 1292 (2001)]

[22] A. Anisovich et al., Eur. Phys. J. A24 (2005) 111

[23] N. Isgur and G. Karl, Phys. Lett. 72B (1977) 109

[24] A.J.G. Hey, P.J. Lichtfield, and R.J. Cashmore, Nucl. Phys. B95 (1975) 516

[25] L.Y. Glozman and D.O. Riska, Phys. Lett. B366 (1996) 305

[26] N. Kaiser, P.B. Siegel, and W. Weise, Phys. Lett. B362 (1995) 23

[27] G. Hoehler, PiN Newslett. 14 (1998) 168

[28] M.F.M. Lutz and E.E. Kolomeitsev, Nucl.Phys. A700 (2002) 193-308

[29] B.Nefkens, πN-newletter 13, 270 (1997)

[30] S. Capstick and W. Roberts, Phys. Rev. D47 (1993) 1994

[31] R. Koniuk and N. Isgur, Phys. Rev. D21 (1980) 1868

[32] S. Capstick and W. Roberts, Phys. Rev D49 (1994) 4570

[33] S. Capstick and W. Roberts, Phys. Rev. D57 (1998) 4301

[34] S. Capstick, Phys. Rev. D46 (1992) 2864

[35] I. Horn, PhD thesis, Rheinische Friedrich-Wilhelms-Universität Bonn, 2004

[36] Ch. Bradtke et al., Nucl. Instr. and Meth. A 436 (1999) 430

[37] Ch. Rohlof and H. Dutz, Nucl. Instr. and Meth. A 526 (2004) 126

[38] W. Roberts and T. Oed, (2004), nucl-th/0410012.

[39] A. Anisovich, E. Klempt, A. Sarantsev, and U. Thoma, Eur. Phys. J. **A24** (2005)

[40] C. Zemach, Phys. Rev. 133 (1964) B1201

[41] C. Zemach, Phys. Rev. 140 (1964) B97

[42] M. Jacob and G.C. Wick, Ann. Phys. 7 (1959) 404

[43] S.U. Chung, Phys. Rev. D48 (1993) 1225

[44] A. Anisovich et al., hep-ph/0407211 (2004)

[45] W. Rarita and J.S. Schwinger, Phys. Rev. 60 (1941) 61

[46] D. Drechsel and L. Tiator, J. Phys. G18 (1992) 449

[47] I.S. Barker et al., Nucl. Phys. B95 (1975) 347

[48] G. Knochlein et al., Z. Phys. A352 (1995) 327

[49] S.U. Chung et al., Phys. Rev. D65 (2002) 072001

[50] C. Amsler, Nucl. Phys. A663 (2000) 93

[51] M. Fuchs, PhD thesis, Rheinische Friedrich-Wilhelms-Universität Bonn, 2005

[52] K. Helbing et al., NIM A 484 (2002) 129

[53] H. Kalinowsky, private communication, 2005